Engineered Cerebral Organoids Recapitulate Adult Tau Expression and Disease-relevant Changes in Tau Splicing

Christopher Lovejoy
University College London https://orcid.org/0000-0001-5125-4383
Argyro Alatza
University College London
Charles Arber
University College London
Grant Galasso
Washington University in Saint Louis
Teisha Y. Bradshaw
University College London
An Verheyen
Janssen Pharmaceutica NV
Tammaryn Lashley
University College London
Tamas Revesz
University College London
John Hardy
University College London
Celeste M. Karch
Washington University in Saint Louis
Selina Wray (selina.wray@ucl.ac.uk)
University College London

Research article

Keywords: Tau, MAPT, frontotemporal dementia, Alzheimer's disease, induced pluripotent stem cells, cerebral organoids, engineered cerebral organoids

Posted Date: June 30th, 2020

DOI: https://doi.org/10.21203/rs.3.rs-37620/v1

Abstract

The tauopathies are a collection of clinically and pathologically diverse neurodegenerative disorders characterised by tau pathology. The tau protein exists as multiple protein isoforms in the adult human CNS, generated by alternative splicing of the *MAPT* gene. Disruptions to tau splicing are associated with a number of tauopathies, however, *in vitro* and *in vivo* models to understand the consequences of disrupted tau splicing have been lacking, due in part to species differences in tau splicing and the developmental regulation of tau in human neurons. We investigated the utility of iPSC-derived cerebral organoids to model key aspects of tau biology. Cerebral organoids showed high variability in neuronal content and tau expression. To reduce this heterogeneity, we generated engineered cerebral organoids (enCORs), which use a floating scaffold to increase the efficiency of neural induction and reduce heterogeneity. We show that enCORs provide a robust and reproducible *in vitro* system for the analysis of tau expression and splicing in a 3D model. To investigate the effect of tau mutations, we generated enCORs from an isogenic series of iPSC with the *MAPT* 10+16 and P301S mutations. The presence of tau splicing mutations results in disease-associated alterations in tau expression, specifically a dose-dependent increase in 4R tau isoforms in the presence of the *MAPT* 10+16 variant. While the developmental regulation of tau splicing is conserved, maturation of tau splicing is accelerated in 3D cultures compared to 2D cultures. Finally, enCORs with coding mutations in *MAPT* are able to produce seed-competent tau species, suggesting enCORs recapitulate early features of tau pathology. In summary, enCORs provide a novel, robust *in vitro* system for the study of tau in development and disease.

Introduction

Hyperphosphorylated, insoluble aggregates composed of the microtubule associated protein tau define a group of clinically and pathologically diverse neurodegenerative diseases collectively called the tauopathies. Tau is primarily known for its a role as a microtubule stabilising protein, although its multifunctional nature is becoming increasingly recognised, with roles in the nucleus andcell signalling (1–3). Tau is present in the adult human CNS as multiple protein isoforms generated by alternative splicing, with either 0, 1 or 2 N-terminal inserts (0N, 1N, 2N) and either 3 or 4 C-terminal repeats (3R, 4R)(4). The precise stoichiometry of tau isoforms is tightly regulated: the levels of 3R and 4R in the adult human CNS are approximately equal, and this appears to have a direct influence on neuronal viability, as mutations in *MAPT* that disrupt tau splicing are causative of frontotemporal dementia and parkinsonism linked to chromosome 17 (FTDP17T) (5,6). Pathological tau aggregates can be composed of all tau isoforms – for example in Alzheimer's Disease – or a subset of tau isoforms, such as progressive supranuclear palsy (PSP), corticobasal degeneration (CBD) and FTD with splice-site mutations in *MAPT*, all of which show a predominant deposition of 4R isoforms(1).

The development of *in vitro* models to study the complex regulation of tau splicing and its involvement in disease requires splicing of *MAPT*that recapitulates the complex patterns of tau protein isoforms seen in the human brain.This has been challenging to the field due to the cell type and species-specific regulation of tau expression, however there are multiple reasons why an *in vitro*, human system with tau expression and splicing patterns that resemble the adult CNS are essential. Although splice-site mutations in *MAPT* were discovered in 1998(5), we know little about the mechanism by which relative increases in certain isoforms can drive neurodegeneration. Recent progress has enabled detailed structures of tau filaments from multiple tauopathies to be resolved using cryo-EM(7–10). This work has shown that distinct tauopathies are characterised by unique structures, which are (in part) a result of the deposition of specific tau isoforms.

The directed differentiation of induced pluripotent stem cells (iPSC) into specific neuronal subtypes provides an unlimited supply of human neurons that can be used to study disease mechanisms. Multiple groups have used this approach to successfully study tauopathies (11). While this is a promising approach, a major challenge is overcoming the developmental regulation of tau; during fetal stages, the 0N3R isoform constitutes the majority of tau(12,13), a phenomenon recapitulated in iPSC-neurons by multiple groups(14,15). Although multiple tau isoforms can be observed in iPSC-neurons, this can require long-term culture (150-365 days) and/or the presence of splice mutations in *MAPT*, and it remains to be determined whether these recapitulate the precise stoichiometry of tau splicing seen in the adult brain (14,16–19).

There is some evidence that culturing cells in 3D may accelerate the appearance of 4R tau isoforms(20,21).A direct comparisonof neurons derived from immortalised neural stem cells that were either cultured in an adherent monolayer or in a 3D suspension in Matrigel showed earlier expression of 4R tau in the 3D cultures(20).In 3D cultures from iPSC-neurons, transcripts for all tau isoforms were detected after 25 weeks(21). Cerebral organoids provide an alternative approach to generate 3D models of neurological disease that are more physiologically relevant in several aspects. By providing a permissive environment for pluripotent cells to differentiate using their intrinsic differentiation cues, organoids contain multiple neuronal subtypes together with some of the physical architecture of the developing brain(22–24). Organoids have been successfully used to model neurodevelopment and are increasingly being used to model neurodegenerative disease(25,26).One of the limitations in the use of cerebral organoids has been the high variability between batches of organoids, with neural induction efficiencies ranging between 30-100% (24). The use ofpoly(lactic-co-glycolic acid)(PGLA) copolymer fibres as floating scaffolds promotes the efficiency of neural induction by providing an optimal surface-to-volume ratio(24). The resulting engineered cerebral organoids (enCORs) have an increased neuronal content, reduced levels of alternative cellular identities, and reduced heterogeneity between batches(24). A detailed investigation of tau expression and splicing in cerebral organoids and enCORs has not yet been described.

Here, we show that cerebral organoids are highly variable in terms of neuronal content and tau expression, whereasenCORs provide a robust and reproducible*in vitro* system for the study of tau expression and splicing. The developmental regulation of tau splicing is preserved in enCORs, however the development of a mature tau isoform signature is accelerated in comparison to 2D cortical neuronal differentiation. Using a previously-described panel of isogenic iPSC(19), we show a dose-dependent effect of the *MAPT* 10+16 mutation on excess of 4R tau expression. Finally, *MAPT* mutation enCORs can induce the seeding of tau aggregation in a tau biosensor assay, suggesting enCORs contain early forms of pathological, seed-competent tau.

Methods

iPSC culture

Control lines used for cerebral organoid generation were described previously [14]. Isogenic iPSC with *MAPT* mutations were generated by Janssen and obtained from EBiSC (https://ebisc.org)(19). iPSC with the following *MAPT* genotypes were used and the EBiSC accession numbers are given in parentheses:WT (SIGi001-A-1), 10+16m mono-allelic (SIGi001-A-13), 10+16bibiallelic (SIGi001-A-12), and 10+16 biallelic/P301S biallelic (SIGi001-A-10).

iPSC lines were cultured in feeder-free conditions on plates coated with Geltrex (Gibco, A14133-02) diluted 1:100 with DMEM/F12 (Gibco, #10565-018). Cultures were fed daily with Essential 8 media (Gibco, #A15169-01, + Supplement, Gibco, #A15171-01) and passaged every 5–7 days using 500μM EDTA (Invitrogen, #15575-038).

Differentiation of iPSC into 2D cortical neurons

Differentiation of iPSC into cortical neurons was performed as described in Shi et al (Shi et al, 2012). Briefly, iPSC lines were grown to 100% confluence before switching to neural induction media, which is N2B27 neuronal maintenance media containing 10μM SB431542 (Tocris) and 1 μMDorsomorphin (R and D systems,#1614/10). N2B27 neuronal maintenance media consisted of a 1:1 mixture of Dulbecco's modified eagle medium F12 and Neurobasal (Gibco, #12348-017) supplemented with 0.5% N2 (Gibco, #17502-048), 1% B27 (Gibco, #17504044), 0.5% non-essential amino acids (NEAA) (Sigma, #M7145), 1 mM L-glutamine (Gibco, #25030081), 25U pen/strep (Gibco, #H4034-100G), 10 μM β-mercaptoethanol (Gibco, #31350-010) and 25U insulin (Sigma, #19278-5ML). Neural induction media was replaced daily, and 10-12 days post-induction the neuroepithelial layer was detached using dispase (Invitrogen,#17105-041), re-plated onto laminin-coated wells (Sigma, #L2020, 1:100 diluted in PBS, Gibco, 10010023) in N2B27 maintenance media without SB43142 and Dorsomorphin. Media was replaced every 3 days and precursors were passaged using dispase onto fresh laminin-coated plates every 5-7 days. The final passage was performed at day 35 using accutase (Gibco #A11105-01), and cells were plated at a final density of 50,000 cells per cm^2 onto plates coated with poly-ornithine (Sigma, #P4957) and laminin, and maintained in N2B27 media until the required timepoint.

Differentiation of iPSC into 3D cerebral organoids

Cerebral organoids were generated using the protocol described by Lancaster et al (27). Briefly, iPSC were detached from plates using EDTA, prior to dissociation into single cells using accutase. Single cells were plated into low attachment round bottomed 96 well plates (CoStar, #7007) at a density of 9000 cells per well in low FGF/standard organoid hESC media: DMEM F12 with the addition of 10% knock out serum replacement (Thermo #10828028), 3% embryonic stem cell quality fetal bovine serum (ESC-Quality FBS) (Invitrogen, #10828-028), 1% GlutaMAX (Invitrogen, #35050-038) , 1% non-essential amino acids (NEAA) and 0.1 mM β-mercaptoethanol, bFGF (Peprotech, #100-18B) at 4ng/mL and 50mM Y-27632 ROCK inhibitor (VWR, #688000-5). Embryoid bodies were fed every 48h. At day 6 the embryoid bodies were transferred to low attachment 24 well plates (Corning, #3473) and induction media added: DMEM F12 with the addition of 1% N2 supplement, 1% NEAA and Heparin (Sigma, #H3149-25KU) to a final concentration of 1μg/mL.

At day 10-12 the neuroepithelial tissues were embedded in 20-30μL of Matrigel (BD Biosciences, #356234) using parafilm moulds and allowed to polymerise at 37°C. The embedded organoids were then placed in a 5cm tissue culture dish (Corning, #430589) containing Cerebral Organoid Differentiation Media (CODM) without Vitamin A: 1:1 ratio of DMEM-F12 Medium and Neurobasal Medium, 0.5% N2 supplement, 0.025% Insulin, 1% GlutaMAX supplement, 0.5% NEAA, 0.5% Penicillin Streptomycin (Gibco, #H4034-100G), 50mM β-mercaptoethanol, 2% of B27 supplement without Vitamin A (Gibco, #12587010).

The media was replaced after 48h with CODM with the addition of vitamin A within the B27 supplement and moved onto an orbital shaker at 55-85 rpm (IKA, #0009019200). Once transferred to the shaker, media was replaced every 3-4 days until the required time point. Phase contrast images of organoids were taken using an Olympus CKX41 phase contrast microscope.

Engineered Cerebral Organoids (enCORs) using iPSC and PLGA fibers

Engineered cerebral organoids (enCORs) were generated according to the protocol described by Lancaster et al (24) . PLGA Vicryl violet sutures (Ethicon, #W9567) were cut into pieces <1mm in length. 5-10 fibres were placed in each well of a 96 well round bottomed low attachment plate. 18,000 iPSC cells (prepared as described above) were seeded per well on top of the fibres. Embryoid bodies were maintained as described above, embedded in Matrigel at day 11-12 but kept in induction media from days 5/6 to days 12/13. Two days post-embedding, the media was changed to Improved Differentiation Media minus vitamin A (IDM-A): 1:1 ratio of DMEM-F12 Medium and Neurobasal Medium, 0.5% N2 supplement, 0.025% Insulin, 1% GlutaMAX supplement, 0.5% NEAA, 0.5% Penicillin Streptomycin, 50mM 2-mercaptoethanol, 2% of B27 supplement without vitamin A. On days 13-16 3mM CHIR99021 (Tocris, #4423) was added to the media.

At day 18-20 enCORs were moved to the orbital shaker at 85rpm, to give them a throw of 10mm. From day 20 onwards Improved Differentiation Media plus Vitamin A & C + HEPES (IDM+vA) was used: a 1:1 mix of DMEM-F12 Medium andNeurobasal Medium, 0.5% N2 supplement, 0.025% Insulin, 1% GlutaMAX supplement, 0.5% NEAA, 0.5% Penicillin Streptomycin, 50mM b-mercaptoethanol, 2% of B27 supplement with Vitamin A, 0.5µg/mL Vitamin C / Ascorbic acid (Sigma, #A4403-100MG), 1.49g HEPES per 500mL (Sigma, #H4034-100G). The media was changed every 3-4 days and 1% Matrigel was added to the media from day 40 onwards. Phase contrast images of organoids were taken using an Olympus CKX41 phase contrast microscope.

Generation of Forebrain Organoids

Forebrain organoids were generated according to the protocol described by Qian et al (28). Briefly, EBs were generated as described in the cerebral organoid protocol, with the addition of 2 µM SB431542 and 2 µMdorsomorphin to the embryoid body media as well as the omission of bFGF. Embryoid bodies were fed every 48h and were not transferred to 24-well plates remaining in the 96-well plates. On day 6 dual SMAD cerebral organoid induction media was added. Similar to the cerebral organoid induction media but with the addition of 1mM SB431542 and 1mM CHIR99021. At day 7 the neuroepithelial tissues were embedded in 20-30µL of Matrigel and embedded organoids were then placed in a 5cm tissue culture dish containing dual SMAD induction media.

The media was replaced at day 14 with CODM with the addition of vitamin A and moved onto an orbital shaker at 55-85 rpm. Once on the shaker the media was replaced every 3-4 days.

Fixation of organoids and preparation of frozen sections

Whole COs and enCORs were fixed in 4% paraformaldehyde for 30 min at RT, washed with PBS and immersed in 30% sucrose overnight at 4°C. Samples were embedded in optimum cutting temperature compound (OCT) and 10 µm sections cut using a cryostat.

Immunocytochemistry

Tissue sections were permeabilised using PBS 0.3% Triton X-100 (PBS-T), blocked with 5% bovine serum albumin (BSA) in PBS-T for 1 hour before incubation with primary antibodies (Table 2) diluted in blocking solution overnight at 4°C. Slides were then washed with PBS-T, incubated with secondary antibodies (Table 4) at 1:1000 concentration for 1h at RT. Following PBS-T washes, nuclei were stained with 4',6-diamidino-2-

phenylindole (DAPI) (Sigma) for 5 mins and then washed with PBS-T. A coverslip was attached to the slide using Fluorescent Mounting Medium (DAKO, #53023) and stored at 4°C.

Slides were imaged using a Leica CTR6000 and Hamamatsu C10600 camera.

SDS-PAGE and Western Blotting

3D or 2D neuronal cultures were lysed in RIPA buffer (10mM Tris-CL, 1mM EDTA, 0.5mM EGTA, 1% Triton X-100, 0.1% Sodium Deoxycholate, 0.1% SDS, 140mM NaCl) or TRIS lysis buffer (25mM Tris-HCL, 0.8M sodium chloride, 1mM EGTA, 50mM imidazole, 25mM beta-glycerophosphate, 20mM sodium fluoride, 10mM sodium pyrophosphate, 0.5mM phenylmethylsulfonyl fluoride). Protease inhibitors (Roche, #11836170001) and phosphatase inhibitors (Roche, #04906845001) were added just before use.Protein concentrations were determined using BCA assay (Biorad), and 4x LDS loading buffer (Invitrogen, #NP0007) supplemented with 20% DTT was added to equal amounts of protein before heating at 98°C for 10 min and centrifugation for 3 minutes at 12000g_{av}. Samples were electrophoresed on 4-12%- SDS-PAGE gels (Invitrogen, #NP0321BOX) at 150V for 3h in running buffer (MES NuPAGE SDS, NOVEX, #NP0002) prior to transfer onto nitrocellulose membrane (GE Healthcare, #10600003) in transfer buffer: H_20 supplemented with 10% Tris/Glycine (Geneflow, #EC-880) and 20% methanol (VWR, #UN1230), for 1hr 15 mins at 30V, blocked in 5%-non-fat milk in PBS with agitation for 1h prior to overnight incubation at 4°C in primary antibody (Table 3) diluted in 5% milk in PBS-T. Membranes were washed with PBS-T before incubation for 1 hour with secondary antibodies (Anti-mouse Alexa Fluor, #A21058 & anti-rabbit Rockland, #611-145-122) diluted (1:20,000) in 5% milk in PBS-T. Secondary antibodies were visualised at 700nm and 800nm using the Li-Cor Odyssey Fc system

Protein dephosphorylation

Dephosphorylation of protein lysates was performed as described previously(29). 10% 10X PMP buffer (New England Biolabs, #B07615), 10% 10mM MnCL2 (New England Biolabs, #B17615) and 4000U l-protein phosphatase (New England Biolabs, #P0753L) was added to equal amount of protein. Samples were vortexed gently for 10 seconds prior to incubation at 30°C for 3h. l-protein phosphatase was inactivated by the addition of LDS-buffer and processing for electrophoresis as described above.

RNA Extraction

Cells and organoids were lysed in 1mL of Trizol (Thermo15596026) and incubated at 4°C with agitation for 20 mins. RNA was extracted from these lysates according to the manufacturers protocol. Briefly, 0.2mL of chloroform was added to the sample, incubated at RT for 2-3 mins and centrifuged at 12,000$g_{(av)}$ at 4°C. Aqueous phase was collected and 0.5mL of isopropanol was added, incubated for 10 mins and centrifuged at 12,000$g_{(av)}$ for 10 mins at4°C. The supernatant was discarded and 1mL 75% ethanol was added and vortexed before centrifugation at 7,500$g_{(av)}$ at 4°C. The supernatant was removed and the pellet was air dried for 10 min at RT. RNA pellets were diluted in 20µL of RNase free water (Ambion, #AM9937) and stored at -80°C. RNA concentration and purity was determined by nanodrop.

Reverse Transcription

1000ng of RNA was reverse transcribed using Super Script IV kit (SSIV, Invitrogen 18090010) according to manufacturer's instructions. Briefly, 1000ng of template RNA was added to RNase free water,2.5mM random hexamers (Invitrogen, #100026484) and 10mM dNTP mix (Invitrogen, #55082, #55083, #55084, #55085) and heated at 65°C for 5mins and then cooled on ice for 1 min. After which SSIV buffer, 100mM DTT, RNaseOUT (Invitrogen, #100000840) and SSIV reverse transcriptase was added to the reaction, heated to 23℃ for 10 mins, incubated at 50-55℃ for 10 mins and finally inactivated by heating at 80°C for 10 mins. The cDNA was then stored at -20°C.

Quantitative PCR

RNA (5mg) was converted to cDNA by PCR using the High-Capacity cDNA Reverse Transcriptase kit (Life Technologies). Taqman real-time PCR assays were utilized to quantify expression for the following genes: exon 10-*MAPT* (Hs00902312_m1); Total *MAPT* (Hs00902194_m1).Samples were run in triplicate with replicate samples analyzed in each plate to control for plate-to-plate variability. To avoid amplification interference, expression assays were run in separate wells from the neuronal housekeeping gene *MAP2*(Hs00258900_m1). Real-time data were analysed by the comparative C_T method. Average C_T values for each sample were normalized to the average C_T values for the neuronal housekeeping gene *MAP2*. The resulting value was then corrected for assay efficiency. Samples with a standard error of 20% or less were subsequently analysed.

Polymerase chain reaction

50ng of cDNA used per reaction with GoTaq Green master mix (Promega #M7123). PCR Reactions were set up according to the manufacturers' protocol. Briefly, 10µL of GoTaq, 9.6µL of H2O, 0.2µM of forward, 0.2µM of reverse primer (Table 1 for primers used and sequences), 50ng template cDNA was added to each reaction. PCR products were separated on a gel composed of 1-2% agarose (Sigma, #A9539) dissolved in 1X TBE (Sigma, #93290) with 1X GelRed (Biotium,#BT41003) alongside a 100 base pair ladder (Bioline, #H4-617110A) at 100V for 1h. PCR products were visualised at 600nm using the Li-Cor Odyssey Fc system.

Tau HEK biosensor cell assay

Tau RD P301S FRET Biosensor cells (ATCC® CRL-3275™) were cultured in DMEM + GlutaMAX (Gibco, #31966-021) with 10% FBS (Gibco, #11573397) and split every 3-5 days using trypsin (Gibco, #25200056). For seeding assays, 115,000 cells were plated on 13mm coverslips (VWR, #631-0148P) in 24 well plates (Thermo, #142485) and left to attach for 24h. Lipofectamine 3000 (Invitrogen, #L3000-001) was used in Opti-MEM (Gibco, 31985062) according to the manufacturers protocol to transfect the Tau RD P301S FRET Biosensor cells with 10ug of enCOR lysate, AD brain lysate, or liposome-only negative control. Cells were fixed with 4% PFA and mounted on to slides before being imaged on confocal microscope. Slides were imaged at 405nm for detection of FRET signal or YFP only at 525-550nm.

Statistical analysis

Densitometric data was obtained from immunoblots using Image Studio software from Licor. GraphPad Prism 8 software was used to implementall statistical analysis of the immunoblot densitometricdata. Information on the number (n) of values used as well as the statistical tests applied can be found in the figure legends.

Results

Generation of cerebral organoids

iPSC from three independent control lines (Ctrl 1, Ctrl2 and Ctrl3) were used to generate cerebral organoidsusing theprotocol developed by Lancaster et al(30) (Fig. 1A). The initial stages of organoid differentiation were monitored by phase contrast microscopy (Fig. 1B). Organoids failing to show translucent neural ectoderm tissue by visual inspection at 14 days *in vitro* (DIV) were discarded.

Cerebral organoids were collected at 30 and 100 DIV for characterisation byimmunocytochemistry (ICC). At 30 DIV, organoids were positive for the neural progenitor cell marker PAX6, radial glial marker phospho-vimentin, the forebrain marker FOXG1, and the deep-layer cortical neuronal marker TBR1 (Fig. 1C).At 100 DIV, organoids were positive for thepan neuronal marker (bIII-tubulin), forebrain marker FOXG1, and the upper layer neuronal marker CTIP2 (Fig. 1D).Together, these results support successful differentiation of iPSC into cerebral organoids.

Cerebral organoidsshow highly heterogeneous tau expression levels

The differentiation of iPSC intocerebral organoids relies onpatterning according to intrinsic signalling, and this therefore can result in substantial heterogeneity between COs(28,31). We wanted to determine whether cerebral organoids would be a suitable system for the analysis of tau isoforms by biochemical assays relying on bulk homogenisation. In order to assess this, we differentiated the 3 independent control iPSC lines into 2D cortical neurons and 3D cerebral organoids. 2D lysates from 3 independent neuronal inductions per control iPSC line, and 3 individual organoids per iPSC line, were analysed by western blotat 80 DIV for total tau, the pan-neuronal marker bIII-tubulin, and the astrocytic marker GFAP(Fig. 2).

2D cortical neuronal cultures showed a robust expression of total tau that was highly consistent between independent inductions as well as between independent control iPSC lines. Neuronal and glial content were assessed by immunoblotting with βIII-tubulin and GFAP levels,respectively and were also consistent across all samples examined (Fig. 2A). In contrast,cerebral organoids showed greater heterogeneity in total tau between independent batches and between cell lines. In the samples with lower tau levels, there also appeared to be lower levels of the pan-neuronal marker βIII-tubulin, suggesting a lower neuronal content in these organoids and consistent with tau expression being predominantly neuronal (Fig. 2B). GAPDH levels were used to demonstrate equal protein loading across samples. Together, these results suggest that cerebral organoids are highly heterogenous and therefore unsuitable for bulk cell biochemical analysis such as western blot.

Generation of engineered cerebral organoids

The high variability between cerebral organoids means analysis of tau expression and splicing is challenging at the protein level. We therefore sought to establish an alternative system that would reduce this heterogeneity. Lancaster et al described a modified protocol to generate engineered cerebral organoids(24) (Fig. 3A). This differs from the original cerebral organoid protocol by the initial seeding of iPSC onto PLGA fibres, permitting theelongation of the EBs andincreasing the surface area to volume ratio. This promotes increased formation of neuroepithelium tissue, and reduced tissue from non-neuronal lineages; therefore increasing homogeneity between individual organoids.PLGA fibresare hydrolysed slowly over a 70day period, eventually leaving the enCORsfree from non-organic components within.

To determine whether this method would reduce the variability in tau expression we previously observed in COs, enCORs were generated from a panel of four isogenic lines, comprising the following *MAPT* genotypes: WT, 10+16 monoallelic (10+16m), 10+16biallelic (10+16bi) and 10+16biallelic/P301Sbiallelic (10+16bi/P301Sbi) (19). Initial differentiation of enCORs was monitored with light microscopy (Fig. 3B) and enCORsthat failed to differentiate were discarded.

enCORs from each genotype were analysed by immunocytochemistry at 30DIV and 100DIV to confirm successful differentiation. Positive immunostaining for markers of forebrain (FOXG1) and deep layer cortical neuronal identity (TBR1) as well as neural precursors (PAX6) and radial glia (phospho vimentin) were observed at 30 DIV in enCORs from all genotypes (Fig. 3B). Further characterisation at 100 DIV (Fig. 3C) confirmed the presence of layer V neuronal markers (CTIP2), forebrain markers (FOXG1), glutamatergic neuronal (VGLUT) and dendritic staining (MAP2), as well as high levels of the pan-neuronal marker staining (βIII-tubulin). Taken together, these data demonstrate successful generation of enCORs and suggest that the presence of 10+16 and P301S *MAPT* mutations do not impair enCOR generation.

EnCORsreduce heterogeneityin tau expression

To determine whether enCORs have robust and reproducible tau expression, we analysed threeindependent batches of 100DIV enCOR lysates from each genotype by western blot (Fig. 4A). A robust and homogenous expression of tau and βIII-tubulin was observed in all organoids examined. Quantification of total tau levels showed no significant difference in tau levels between genotypes (Fig. 4B), and quantification of βIII-tubulin levelsshowed no differences in the levels of the pan-neuronal marker, suggesting reproducible neuronal content between organoids (Fig. 4C). These data suggests enCORs provide an organoid system more suited to bulk population, biochemical readouts, due to reduced variability compared to cerebral organoids.

Next, we investigated tau splicing in enCORs from WT, 10+16m, 10+16bi and 10+16bi/P301Sbi genotypes. The expression of 0N, 1N and 2N *MAPT* isoforms was assessed by RT-PCR using primers spanning exons 1 – 5 (Fig. 4D). RNA from post-mortem brain was used as a positive control, and bands of 112bp (0N), 199bp (1N) and 286bp (2N) could be seen following separation by electrophoresis. As expected, 1N was the most predominant isoform in brain-derived cDNA followed by 0N and 2N(12,15,21). In contrast, the band corresponding to 0N tau was the most predominant in enCORs of all genotypes at 100 DIV, consistent with a predominant expression of 0N isoforms during early development(12,32). A faint band corresponding to 1N tau isoforms could also be observed, and in some enCORs a faint 2N band could be seen, although this was variable. The presence of the 10+16 and P301S *MAPT* mutations did not affect N-terminal splicing.

Next, we investigated the expression of 3R and 4R tau isoforms using primers that span exon 10of *MAPT*, resulting intwo products depending on the exclusion (3R, 305bp) or inclusion (4R, 398bp) of exon 10. In human brain, these two bands were of approximately equal intensity, consistent with an equimolar ratio of 3R:4R isoforms. In WTenCORs, a robust expression of 3R transcripts could be detected by RT-PCR, with only a faint band corresponding to 4R transcripts, suggesting enCORs predominantly express the 0N3R tau isoformup until 100 DIV, consistent with fetal tau profiles previously described in iPSC-derived systems. In contrast, enCORs with the 10+16 mutation have a robust expression of both 3R and 4R transcripts, and the mutation appears to drive 4R expression in a dose-dependent manner.

We then determined tau isoform expression at the protein level by western blot (Fig. 4E). Lysates from 100 DIVenCORs of each genotype were treatedwith λ-phosphatase prior to electrophoresis alongside a recombinant tau ladder with all six tau isoforms. A single band was observed in WTenCORs, corresponding to0N3R tau. EnCORs with the 10+16 mutation expressed both 0N3R tau and 0N4R, as previously shown in 2D(14,19).

These results demonstrate that enCORs provide a system for the investigation of tau expression and splicing with high homogeneity between individual organoids, as well as between batches of organoids. However, in agreement with previous studies of 2D neurons, the tau profile most closely resembles fetal neurons. We therefore investigated tau splicing in enCORsafter extended *in vitro* culture to determine whether the acquisition of mature tau splicing is accelerated in enCORs compared with existing *in vitro* models.

Tau isoform diversity increases in enCORs with extended *in vitro* culture

To systematically investigate when maturation of tau splicing occurs in enCORs, we investigated tau expression and splicing at 200 DIV (Fig. 5) and 300 DIV (Fig. 6). *MAPT*splicing was analysed at the RNA level as described previously for 100 DIV. Assessment of exon 2 and 3 inclusion revealed that multiple N-terminal isoforms are present in enCORs of all genotypes after 200 DIV (Fig. 5A), however variability between enCORs was observed. In contrast to what was observed at 100 DIV, 3R and 4R transcripts were detected in enCORs of all genotypes at 200 DIV. In WTenCORs, bands of approximately equal intensity could be observed, suggesting equal levels of 3R and 4R tau isoforms. The presence of the 10+16 mutation in both mono and biallelic forms increased exon10 inclusion and the relative levels of 4R tau, as expected. This suggests a progression towards mature tau splicing at this time point, at least at the mRNA level.

We next determined if these alterations in tau splicing are also apparent at the protein level. Whole cell lysates from enCORs at 200 DIV were treated (+) and untreated (-) with λ-phosphatase before analysis by western blot (Fig. 5B). In contrast to 100DIV, multiple tau isoforms could now be observed in organoids from all genotypes. 0N3R was still the predominant isoform in control organoids, however high exposure revealed the presence of additional tau isoforms. In organoids with the 10+16 mutation, an increase in 4R tau isoforms was observed in a manner consistent with increased allelic dosage of the mutation.

Tau splicing reaches full maturity by 300 DIV

Although the appearance of multiple tau isoforms was apparent at 200 DIV, we wanted to determine if tau profiles matured further with continued culture to resemble the adult human brain. RNA and protein was extracted from enCORs at 300 DIV for analysis of tau expression and splicing. Equal levels of 3R and 4R tau transcripts were detected in control enCORs, and a relative increase of 4R tau was present in the enCORs with the 10+16 mutation (Fig. 6A). 0N, 1N and 2N tau isoforms were also detected in all enCORs, and in some samples 1N isoforms were the most predominant, consistent with tau expression in the adult human brain. These changes were also confirmed at the protein level (Fig. 6B). Multiple tau isoforms were observed in lines of all genotypes and increased 4R tau was present in enCORs with the 10+16m and 10+16bi genotypes.

Interestingly, 10+16bienCORs now produced nearly all 4R tau with very little 3R tau. In enCORs with both 10+16bi-allelic and P301S bi-allelic mutations, predominantly 0N3R and 0N4R tau isoforms were detected. This is unexpected, given the almost complete reprogramming to 4R seen in enCORs with the 10+16bigenotype, and suggests that the P301S mutation may affect the stability of the 4R tau protein within enCORs.

To exclude the possibility that this maturation in tau splicing is specific to enCORs, we also determined tau isoform expression in organoids generated using a directed differentiation protocol that generates organoids of forebrain identity(33) . Similar splicing patterns were observed in forebrain organoids to enCORs (Fig. 6C and 6D), suggesting this is not an enCOR specific phenomenon. Finally, we wanted to determine if mature tau isoform expression occurs more rapidly in 3D than 2D. RNA and protein lysates from enCORs, forebrain organoids and 2D cortical neurons after 300DIV showed a robust expression of 3R and 4R at the RNA level (Fig. 6E). Further, expression of 1N and 2N within the organoid models was more similar to the human brain sample, compared with 2D cortical neurons. Western blots further uncovered a more complex pattern of tau expression in 3D cultures than 2D (Fig. 6F), consistent with accelerated acquisition of mature tau splicing in these cultures and expression patterns resembling those in the human brain.

enCORs with 10+16bi/P301Sbi produce seed-competent tau species

In order to investigate whether enCORs with *MAPT* mutations develop early signs of tau pathology, we tested whether lysates generated from enCORs contained species competent to induce tau seeding using an established tau biosensor assay(34,35). Previous reports have indicated that the formation of seed-competent tau precedes tangle development, and so we reasoned that this would be a marker of early-stage pathology in our model system(36). Tau RD P301S Biosensor cells were treated with 10ug of 300 DIV enCOR lysates from all genotypes. Brain homogenate from an Alzheimer's disease case was used as a positive control. To assess the presence of tau aggregates, cells were fixed 72h post-transfection and YFP fluorescence was imaged at 527nm. Widespread tau aggregates could be observed in the cells transfected with AD brain lysate. No aggregation was observed in the lipofectamine-only negative control. In the enCOR lysate seeded cells, no tau aggregation was observed for WT, 10+16m and 10+16bi. In contrast, seeding with 10+16bi/P301Sbi lysates resulted in infrequent but distinct inclusions. This could be due to the presence of seed-competent tau species withinenCORs of this genotype that are capable of inducing tau seeds.

Discussion

Here, we provide the first thorough investigation of tau expression and splicing in cerebral organoids.Cerebral organoids are self-organising in vitro tissue models that recapitulate early stages of development and provide a physiologically relevant *in vitro* system for the study of development and disease(30). We show here that cerebral organoids express fetal tau when analysed at 100 DIV, however the high variability between organoids makes biochemical analysis challenging. To address this, we used enCORs, which combine bioengineering and organoid culture to enhance the efficiency of neural induction and reduce heterogeneity(24). enCORs robustly and reproducibly express tau, and model developmental changes to tau splicing.Isogenic iPSC with *MAPT* mutations did not impair organoid differentiation, and the presence of the 10+16 splice site mutation led to an early and increased 4R tau expression in a dose-dependent manner. enCORs reach a human brain-like tau profile at 300 DIV, quicker than what is observed in 2D cortical cultures. Finally, we have shown that enCORsexpressing 10+16 and P301S mutations on both alleles contain seed-competent tau species, capable of inducing inclusion formation in a tau biosensor seeding assay.

Disruptions to tau splicing are present in multiple tauopathies, but*in vitro* models recapitulating human tau splicing have been lacking in the field.iPSC-neurons provide a means to overcome this, but they have been challenging due to the developmental regulation of tau splicing(12,14,19). Transcriptomic studies have shown

iPSC-neurons closely resemble fetal neurons, and multiple reports have shown that the fetal tau isoform (0N3R) is predominantly expressed in these cells, including a quantitative study demonstrating that although 4R tau could be detected by mass spectrometryafter 6-9 weeks of culture, its levels were 100 fold less than in human brain(15).

Although predominantly used as models of development, the potential of cerebral organoids as models of neurodegeneration is emerging(26,37–39). One barrier to their use is the heterogeneity between organoids, as patterning is largely reliant on intrinsic signalling within each organoid. We demonstrated here that substantial variability in tau expression exists in COs, which is likely to be a reflection of the neuronal content of a particular organoid. However, this variability makes biochemical analysis at the bulk population level difficult to interpret.

Newer protocols havereduced this heterogeneity through the use of scaffolds to increase the surface area and subsequent availability of cells to the pro-neural media(24). This reduces heterogeneity as well as minimising the necrotic core described in COs(24,27). Here, we showed that tau expression in enCORs is remarkably consistent between batches, between lines and between organoids within a batch, enhancing their suitability for analysis by biochemical means.

The developmental regulation of tau splicing is conserved in enCORs, as previously described in 2D iPSC-neurons(14,15). However, we observed maturation of tau splicing was accelerated in enCORs compared to our previous results in 2D cortical neurons(14).After 100 DIV, the presence of 4R tau and N-terminal splice variants could be observed at the RNA level in enCORs.This is consistent with previous reports showing accelerated tau maturation in complementary 3D systems(20,21). However, these tau profiles are still immature with respect to the complex patterns observed in the adult human brain. Further diversity in tau isoform expression could be observed at 200 DIV, and at 300 DIV, tau splicing profiles at both the RNA and protein level resembled patterns observed in the adult human brain. A direct comparison of 2D and 3D cultures clearly showed increased diversity of tau isoforms in 3D organoid cultures. Importantly, the maturation of tau splicing was also observed in a second organoid protocol, using inductive conditions to pattern forebrain organoids. To our knowledge, this is the first description of tau splicing in organoid models, and these data are consistent with previous studies that have demonstrated the expression of multiple tau isoforms in other 3D culture systems. Choi et al used neurons derived from immortalised neural precursor cells, and after 7 weeks differentiation observed increased 4R tau transcripts in 3D compared with the same cells cultured in 2D(20). A second study used iPSC-neurons coated on alginate beads, and detected transcripts from all tau isoforms after 25 weeks of differentiation, although 0N3R was still the predominant tau species (75%+ of total tau) (21).Another recent study compared tau expression in cerebral organoids with fetal brain, although they only assessed the location of tau transcripts using RNA scope and no assessment of tau splicing was undertaken (40). The *MAPT* 10+16 mutation had a dramatic effect on tau splicing after 300 DIV, resulting in a near-complete conversion to 4R tau when present in a biallelic form. Although this mutation doesn't exist in patient in the homozygous state, the isogenic series of 10+16m and 10+16bi lines provide new models for the investigation of disrupted tau splicing.

Thus, enCORs provide a robust system to probe the physiological and disease-related regulation of tau splicing. Although the maturation described here is accelerated in comparison to 2D, extended culture times are still required to acquire a profile similar to the adult human brain. This is consistent with genome-wide transcriptomic studies showing the fetal identity of organoids(22). However, the use of non-adherent organoids has benefits at the practical level, as a major risk to long-term 2D cultures is the spontaneous detachment from

cell culture plates. Further, the technology is continually evolving, for example through the development of vascularised organoids(41,42) and slice cultures which enable the formation of distinct cortical layers(43). Thus, further acceleration of organoid maturity is likely to be possible in the future.

It is important to note that organoids are composed of multiple cell types, and our bulk population analysis cannot rule out that early 4R expression is driven by the presence of a specific subpopulation of neurons. Further, both 2D and 3D protocols also result in the generation of astrocytes which will influence neuronal maturity and potentially tau splicing, and although we assessed astrocyte contribution within our organoids, a thorough characterisation of astrocyte function and maturity in 2D versus 3D is warranted. A previous report utilised cortical spheroids to determine that cultured astrocytes did not reach full maturity until around 20 months *in vitro*(44). Although challenging from a practical level, these long-term culture experiments afford opportunities to assess the temporal emergence of cellular phenotypes, as previously shown in iPSC models of Parkinson's Disease, where lysosomal and mitochondrial phenotypes emerged at 70 DIV and 150 DIV respectively(45).

The presence of tau tangles within organoids from iPSC with *MAPT* mutations is yet to be established, however Gallyas positive tau tangles have been described in 3D culture of human neurons overexpressing APP and PSEN1(46), as well as organoids from individuals with mutations in APP and PSEN1(47). The same iPSC lines used in this study were previously used in 2D, and tau aggregation could only be detected after 5 weeks following the addition of exogenous tau seeds(19). We opted to determine whether tau mutations enCORs produced seed-competent tau species, conformers of tau that are sufficient to induce tau aggregation (36).We observed no seeding activity in cell lysates fromWT, 10+16m or 10+16bi organoids, however lysate from 10+16bi/P301Sbi organoids was able to induce tau inclusions. This points towards the early formation of seeds within these cultures and indicates the capability of enCORs to be effective models for investigating the early stages of protein aggregation and seed formation. The tau species responsible for this seeding activity remain to be determined, however it is interesting that the increased ratio in 4R to 3R tau in 10+16 monoallelic and biallelicenCORs is not sufficient to drive seeding in this assay. This finding could mean that the presence of the P301S mutation is required for homotypic seeding.

Conclusion

This study establishes the feasibility of iPSC-organoids as a model for the study of tau expression and splicing. Specifically, we have shown thatenCORs can be used to model developmental and disease-relevant aspects of tau biology, particularly tau splicing. enCORs provide a robust and reproducible *in vitro* model for biochemical analysis of tau, with mature splicing patterns resembling those of the human brain. These advanced 3D culture systems will be important for our understanding of how alterations to tau splicing manifest in neurodegeneration.

List Of Abbreviations

3R tau – Tau with 3 microtubule binding repeats

4R tau – Tau with 4 microtubule binding repeats

0N tau – Tau with 0 N-terminal insert

1N tau - Tau with 1 N-terminal insert

2N tau - Tau with 2 N-terminal insert

2D – Two dimensional

3D – Three dimensional

10+16m – 10+16 monoallelic

10+16bi - 10+16 biallelic

10+16bi/P301Sbi - 10+16biallelic/P301Sbiallelic

AD – Alzheimer's disease

APP – Amyloid precursor protein

B27 – B27 supplement

bFGF – Basic fibroblast growth factor

BRN2 - POU class 3 homeobox 2

BSA - Bovine serum albumin

CO – Cerebral organoid

CBD – Corticobasal degeneration

cDNA - Complementary DNA

CFP – Cyan fluorescent protein

CHIR - CHIR99021

cm - Centimetre

CNS – Central nervous system

CODM – Cerebral organoid differentiation media

CTIP2 - Bcl11b

DAPI - 4',6-diamidino-2-phenylindole

DIV – Days in vitro

DTT - Dithiothreitol

DMEM - Dulbecco's modified eagle medium

DM - Dorsomorphin

DNA – Deoxyribonucleic acid

dNTP - Deoxynucleotide

DSO – Dual-SMAD organoid

E8 – Essential 8 media

EB – Embryoid body

EDTA - Ethylenediaminetetraacetic acid

EGTA - Ethylene glycol tetraacetic acid

EM – Electron microscopy

enCOR – Engineered cerebral organoid

ESC-Quality FBS - ESC-Quality FBS

FBS – Fetal bovine serum

FOXG1 - Forkhead box G1

FRET - Förster resonance energy transfer

FTD - Frontotemporal dementia

FTDP17T - Frontotemporal dementia and parkinsonism linked to chromosome 17

GAPDH - Glyceraldehyde 3-phosphate dehydrogenase

GFAP - Glial fibrillary acidic protein

h - Hour

HEPES - 4-(2-hydroxyethyl)-1-piperazineethanesulfonic acid

ICC – Imunnocytochemistry

IDM-A – Improved differentiation media minus vitamin A

IDM+vA - Improved Differentiation Media plus Vitamin A & C + HEPES

iPSC – Induced pluripotent stem cells

Ki67 - Antigen KI-67

LDS - Laemmli sample buffer

MAP2 - Microtubule associated protein 2

MAPT - Microtubule associated protein tau

min – Minute

MTBR – Microtubule binding repeat

N2 – N2 suppliment

N2B27 - Neuronal maintenance media

NEAA – Non-essential amino acids

NPC – Neural precursor cell

OCT - Optimum cutting temperature compound

PAX6 - Paired box protein Pax-6

PBS - Phosphate buffered saline

PBS-T - Phosphate buffered saline + triton X-100

PCR – Polymerase chain reaction

PFA - Paraformaldehyde

PLGA - poly(lactic-co-glycolic acid)

PMP - Protein metallo phosphatases buffer

PSEN1 - Presenilin-1

PSP - Progressive supranuclear palsy

qPCR – Quantitative polymerase chain reaction

rpm – Revolutions per minute

RNA - Ribonucleic acid

RT – Room temperature

RT-PCR – Reverse transcription polymerase chain reaction

SB - SB431542

SSIV – Superscript IV

TBR1 - T-box brain transcription factor 1

V - Volts

VGULT - Glutamate vesicular transporter

WT – Wild type

YFP – Yellow fluorescent protein

Declarations

Acknowledgements

This work was funded by the Joy Bunker PhD scholarship (CL, SW), an Alzheimer's Research UK Senior Research Fellowship (SRF2016B-2, SW; SRF2015-2, TL), and the NIHR Queen Square Biomedical Research Centre. The views expressed are those of the authors and not necessarily those of the NHS, the NIHR or theDepartment of Health. JH is funded by the UK Dementia Research Institute which receives its funding from DRI Ltd, funded by the UK Medical Research Council, Alzheimer's Society and Alzheimer's Research UK, Medical Research Council (award number MR/N026004/1), the Wellcome Trust (award number 202903/Z/16/Z), and the Dolby Family Fund. CA is funded by an Alzheimer's Society Research Fellowship(AS-JF-18-008). CMK and GG are funded by the Farrell Family Alzheimer's Disease Research Fund, the Rainwater Charitable Organization and NIH R56 NS110890.TR and SW are recipients of a grant from the Karin &StenMortstedt CBD Solutions, which supports TB (Grant code: 512385). The Queen Square Brain Bank is supported by the Reta Lila Weston Institute of Neurological Studies, UCL Institute of Neurology.We thank Janssen for the provision of iPSC used in this study.

Author contributions

Conceptualization: SW, JH. Methodology: CL, SW, CA, AA, GG, TYB. Investigation: CL, CA, AA, GG, CMK, SW. Writing - Original draft: SW, CL, CA, CMK. Writing-review and editing: CL, CA, TL, TR, JH, CMK, SW. Resources: AV, TL, TR. Funding acquisition: SW, JH. All authors read and approved the final manuscript.

References

1. Guo T, Noble W, Hanger DP. Roles of tau protein in health and disease. Acta Neuropathol. 2017;
2. Surridge CD, Burns RG. The Difference in the Binding of Phosphatidylinositol Distinguishes MAP2 from MAP2C and Tau1" [Internet]. Vol. 33, Biochemistry. 1994
3. Maina MB, Al-Hilaly YK, Serpell LC. Nuclear tau and its potential role in alzheimer's disease. Biomolecules. 2016;6(1):2–20.
4. Andreadis A. Tau splicing and the intricacies of dementia [Internet]. Vol. 227, Journal of Cellular Physiology. 2012 [cited 2018 Sep 13]. p. 1220–5.
5. Hutton M, Lendon CL, Rizzu P, Baker M, Froelich S, Houlden H, et al. Association of missense and 5-splice-site mutations in tau with the inherited dementia FTDP-17. 1998 [cited 2019 Feb 6].

6. Poorkaj P, Bird TD, Wijsman E, Nemens E, Garruto RM, Anderson L, et al. Tau is a candidate gene for chromosome 17 frontotemporal dementia. Ann Neurol [Internet]. 1998 Jun [cited 2020 Apr 22];43(6):815–25.
7. Falcon B, Zivanov J, Zhang W, Murzin AG, Garringer HJ, Vidal ruben, et al. Novel tau filament fold in chronic traumatic encephalopathy encloses hydrophobic molecules. [cited 2020 Apr 16]; Available from: https://doi.org/10.1038/s41586-019-1026-5
8. Zhang W, Tarutani A, Newell KL, Murzin AG, Matsubara T, Falcon B, et al. Novel tau filament fold in corticobasal degeneration. Nature [Internet]. 2020 [cited 2020 Apr 16];580(7802):283–7. Available from: https://doi.org/10.1038/s41586-020-2043-0
9. Falcon B, Zhang W, Murzin AG, Murshudov G, Garringer HJ, Vidal R, et al. Structures of filaments from Pick's disease reveal a novel tau protein fold. 2018 [cited 2019 Feb 20]; Available from: https://doi.org/10.1038/s41586-018-0454-y
10. Fitzpatrick AWP, Falcon B, He S, Murzin AG, Murshudov G, Garringer HJ, et al. Cryo-EM structures of tau filaments from Alzheimer's disease. Nature [Internet]. 2017;547(7662):185–90. Available from: http://dx.doi.org/10.1038/nature23002
11. Wray S. Modeling tau pathology in human stem cell derived neurons. Brain Pathol. 2017;27(4):525–9.
12. Hefti MM, Farrell K, Kim SH, Bowles KR, Fowkes ME, Raj T, et al. High-resolution temporal and regional mapping of MAPT expression and splicing in human brain development. PLoS One. 2018;13(4):1–14.
13. Goedert M, Spillantini MG, Jakes R, Rutherford D, Crowther RA. Multiple isoforms of human microtubule-associated protein tau: sequences and localization in neurofibrillary tangles of Alzheimer's disease. Neuron. 1989;3(4):519–26.
14. Sposito T, Preza E, Mahoney CJ, Setó-Salvia N, Ryan NS, Morris HR, et al. Developmental regulation of tau splicing is disrupted in stem cell-derived neurons from frontotemporal dementia patients with the 10 + 16 splice-site mutation in MAPT. Hum Mol Genet [Internet]. 2015 [cited 2019 Feb 6];24(18):5260–9. Available from: https://www.ncbi.nlm.nih.gov/pmc/articles/PMC4550814/pdf/ddv246.pdf
15. Sato C, Barthélemy NR, Mawuenyega KG, Patterson BW, Gordon BA, Jockel-Balsarotti J, et al. Tau Kinetics in Neurons and the Human Central Nervous System. Neuron [Internet]. 2018;97(6):1284-1298.e7. Available from: http://linkinghub.elsevier.com/retrieve/pii/S0896627318301363
16. Imamura K, Sahara N, Kanaan NM, Tsukita K, Kondo T, Kutoku Y, et al. Calcium dysregulation contributes to neurodegeneration in FTLD patient iPSC-derived neurons. 2016 [cited 2019 Mar 5]; Available from: www.nature.com/scientificreports
17. Iovino M, Agathou S, González-Rueda A, Del Castillo Velasco-Herrera M, Borroni B, Alberici A, et al. Early maturation and distinct tau pathology in induced pluripotent stem cell-derived neurons from patients with MAPT mutations. Brain [Internet]. 2015 [cited 2019 Feb 26];138(11):3345–59. Available from: https://www.coriell.org/
18. Wren MC, Zhao J, Liu C-C, Murray ME, Atagi Y, Davis MD, et al. Frontotemporal dementia-associated N279K tau mutant disrupts subcellular vesicle trafficking and induces cellular stress in iPSC-derived neural stem cells. Mol Neurodegener [Internet]. 2015 Sep 15 [cited 2019 Feb 23];10:46. Available from: http://www.ncbi.nlm.nih.gov/pubmed/26373282
19. Verheyen A, Diels A, Reumers J, Van Hoorde K, Van den Wyngaert I, van Outryve d'Ydewalle C, et al. Genetically Engineered iPSC-Derived FTDP-17 MAPT Neurons Display Mutation-Specific Neurodegenerative

and Neurodevelopmental Phenotypes. Stem Cell Reports [Internet]. 2018 Aug [cited 2019 Feb 25];11(2):363–79. Available from: https://linkinghub.elsevier.com/retrieve/pii/S2213671118302856

20. Choi SH, Kim YH, Hebisch M, Sliwinski C, Lee S, D'Avanzo C, et al. A three-dimensional human neural cell culture model of Alzheimer's disease. Nature [Internet]. 2014;515(7526):274–8. Available from: http://www.ncbi.nlm.nih.gov/pubmed/25307057%5Cnhttp://www.pubmedcentral.nih.gov/articlerender.fcgi?artid=PMC4366007
21. Miguel L, Rovelet-Lecrux A, Feyeux M, Frebourg T, Nassoy P, Campion D, et al. Detection of all adult Tau isoforms in a 3D culture model of iPSC-derived neurons. Stem Cell Res [Internet]. 2019 Oct [cited 2019 Sep 16];40:101541. Available from: https://linkinghub.elsevier.com/retrieve/pii/S1873506119301710
22. Camp JG, Badsha F, Florio M, Kanton S, Gerber T, Wilsch-Bräuninger M, et al. Human cerebral organoids recapitulate gene expression programs of fetal neocortex development. Proc Natl Acad Sci U S A [Internet]. 2015;112(51):15672–7. Available from: http://www.pubmedcentral.nih.gov/articlerender.fcgi?artid=4697386&tool=pmcentrez&rendertype=abstract
23. Di Lullo E, Kriegstein AR. The use of brain organoids to investigate neural development and disease. Nat Rev Neurosci [Internet]. 2017;18(10):573–84. Available from: http://www.nature.com/doifinder/10.1038/nrn.2017.107
24. Lancaster MA, Corsini NS, Wolfinger S, Gustafson EH, Phillips AW, Burkard TR, et al. Guided self-organization and cortical plate formation in human brain organoids. Nat Biotechnol [Internet]. 2017 [cited 2017 Jun 28];35(7):659–66. Available from: https://www.nature.com/nbt/journal/vaop/ncurrent/pdf/nbt.3906.pdf
25. Benito-Kwiecinski S, Lancaster MA. Brain Organoids: Human Neurodevelopment in a Dish. Cold Spring Harb Perspect Biol. 2019;a035709.
26. Grenier K, Kao J, Diamandis P. Three-dimensional modeling of human neurodegeneration: brain organoids coming of age. Mol Psychiatry [Internet]. 2019 [cited 2019 Aug 28]; Available from: https://doi.org/10.1038/s41380-019-0500-7
27. Madeline A. Lancaster JAK. Generation of Cerebral Organoids from Human Pluripotent Stem Cells. Adv Mater Process [Internet]. 2014 [cited 2017 Apr 20];148(5):29–30. Available from: https://www.ncbi.nlm.nih.gov/pmc/articles/PMC4160653/pdf/emss-60322.pdf
28. Qian X, Nguyen HN, Song MM, Hadiono C, Ogden SC, Hammack C, et al. Brain-Region-Specific Organoids Using Mini-bioreactors for Modeling ZIKV Exposure. Cell [Internet]. 2016;165(5):1238–54. Available from: http://dx.doi.org/10.1016/j.cell.2016.04.032
29. Hanger D., Gibb G., de Silva R, Boutajangout A, Brion J-P, Revesz T, et al. The complex relationship between soluble and insoluble tau in tauopathies revealed by efficient dephosphorylation and specific antibodies. FEBS Lett [Internet]. 2002 Nov 20 [cited 2020 Apr 22];531(3):538–42. Available from: http://doi.wiley.com/10.1016/S0014-5793%2802%2903611-6
30. Lancaster MA, Hurles ME, Homfray T, Bicknell LS, Jackson AP, Martin C-A, et al. Cerebral organoids model human brain development and microcephaly. Nature [Internet]. 2013 Aug 28 [cited 2016 Dec 19];501(7467):373–9. Available from: http://www.nature.com/doifinder/10.1038/nature12517
31. Sun AX, Ng HH, Tan EK. Translational potential of human brain organoids. Ann Clin Transl Neurol. 2018;5(2):226–35.
32. Takuma H, Arawaka S, Mori H. Isoforms changes of tau protein during development in various species. Dev Brain Res. 2003;

33. Qian X, Nguyen HN, Song MM, Hadiono C, Ogden SC, Hammack C, et al. Brain-Region-Specific Organoids Using Mini- bioreactors for Modeling ZIKV Exposure Brain-Region-Specific Organoids Using Mini-bioreactors for Modeling ZIKV Exposure. Cell [Internet]. 2016 [cited 2017 Jun 26];165:1238–54. Available from: http://dx.doi.org/10.1016/j.cell.2016.04.032
34. Holmes BB, Furman JL, Mahan TE, Yamasaki TR, Mirbaha H, Eades WC, et al. Proteopathic tau seeding predicts tauopathy in vivo. [cited 2020 Apr 16]; Available from: www.pnas.org/cgi/doi/10.1073/pnas.1411649111
35. Kaufman SK, Thomas TL, Tredici K Del, Braak H, Diamond MI. Characterization of tau prion seeding activity and strains from formaldehyde-fixed tissue.
36. DeVos SL, Corjuc BT, Oakley DH, Nobuhara CK, Bannon RN, Chase A, et al. Synaptic tau seeding precedes tau pathology in human Alzheimer's disease brain. Front Neurosci. 2018 Apr 24;12(APR).
37. Amin ND, Paşca SP. Building Models of Brain Disorders with Three-Dimensional Organoids [Internet]. Vol. 100, Neuron. 2018 [cited 2018 Dec 19]. p. 389–405. Available from: https://linkinghub.elsevier.com/retrieve/pii/S089662731830895X
38. Faravelli I, Costamagna G, Tamanini S, Corti S. Back to the origins: Human brain organoids to investigate neurodegeneration. Vol. 1727, Brain Research. Elsevier B.V.; 2020.
39. Raja WK, Mungenast AE, Lin Y-T, Ko T, Abdurrob F, Seo J, et al. Self-Organizing 3D Human Neural Tissue Derived from Induced Pluripotent Stem Cells Recapitulate Alzheimer's Disease Phenotypes.
40. Fiock KL, Smalley ME, Crary JF, Pasca AM, Hefti MM. Increased Tau Expression Correlates with Neuronal Maturation in the Developing Human Cerebral Cortex. eneuro [Internet]. 2020 [cited 2020 Jun 3];ENEURO.0058-20.2020. Available from: https://doi.org/10.1523/ENEURO.0058-20.2020
41. Mansour AA, Gonçalves JT, Bloyd CW, Li H, Fernandes S, Quang D, et al. An in vivo model of functional and vascularized human brain organoids. Nat Biotechnol [Internet]. 2018;(April). Available from: http://www.nature.com/doifinder/10.1038/nbt.4127
42. Cakir B, Xiang Y, Tanaka Y, Kural MH, Parent M, Kang Y-J, et al. Engineering of human brain organoids with a functional vascular-like system. Nat Methods [Internet]. [cited 2020 Feb 12]; Available from: https://doi.org/10.1038/s41592-019-0586-5
43. Qian X, Su Y, Adam CD, Deutschmann AU, Pather SR, Goldberg EM, et al. Sliced Human Cortical Organoids for Modeling Distinct Cortical Layer Formation. Cell Stem Cell [Internet]. 2020; Available from: http://www.ncbi.nlm.nih.gov/pubmed/32142682
44. Sloan SA, Darmanis S, Huber N, Khan TA, Birey F, Caneda C, et al. Human Astrocyte Maturation Captured in 3D Cerebral Cortical Spheroids Derived from Pluripotent Stem Cells. Neuron. 2017;95(4):779-790.e6.
45. Burbulla LF, Song P, Mazzulli JR, Zampese E, Wong YC, Jeon S, et al. Dopamine oxidation mediates mitochondrial and lysosomal dysfunction in Parkinson's disease. Science (80-). 2017;357(6357):1255–61.
46. Park J, Wetzel I, Marriott I, Dréau D, D'Avanzo C, Kim DY, et al. A 3D human triculture system modeling neurodegeneration and neuroinflammation in Alzheimer's disease. Nat Neurosci [Internet]. 2018 [cited 2018 Jul 2];21(7):941–51. Available from: https://www.nature.com/articles/s41593-018-0175-4.pdf
47. Gonzalez C, Armijo E, Bravo-Alegria J, Becerra-Calixto A, Charles •, Mays E, et al. Modeling amyloid beta and tau pathology in human cerebral organoids. 2018 [cited 2018 Sep 3]; Available from: https://doi.org/10.1038/s41380-018-0229-8

48. Wolozin BL, Pruchnicki A, Dickson DW, Davies P. A neuronal antigen in the brains of Alzheimer patients. Science (80-) [Internet]. 1986 [cited 2019 Feb 20];232(4750):648–50. Available from: http://science.sciencemag.org/content/232/4750/648#BIBL

Tables

Table 1.
Primers used in this study

Primer	Sequence 5' to 3'	Product Length		
9-13 R Tau Forward	GTCAAGTCCAAGATCGGCTC	3R – 305bp	4R - 398bp	
9-13 R Tau Reverse	TGGTCTGTCTTGGCTTTGGG			
2-3-4 N Tau Forward	TACGGGTTGGGGGACAGGAAACAT	0N - 112bp 286bp	1N - 199bp	2N -
2-3-4 N Tau Reverse	GGGGTGTCTCCAATGCCTGCTTCT			
2-3 N Tau Forward	TGAACCAGGATGGCTGAGC	0N - 254bp 428bp	1N - 341bp	2N -
2-3 N Tau Reverse	TTGTCATCGCTTCCAGTCC			
GAPDH Forward	CCATGGCACCGTCAAGGCT	469bp		
GAPDH Reverse	GCCAGTAGAGGCAGGGATG			

Table 2.
Primary antibodies used in this study for immunofluorescence

Name / Target	Species	Product Code	Company	Dilution
Sox2	Rabbit	AB5603	Millipore	1:300
Tbr2	Rabbit	AB2283	Millipore	1:200
Foxg1	Rabbit	ab18259	Abcam	1:400
Phospho- vimentin	Mouse	D076-3S	MBL International	1:250
βIII-tubulin	Rabbit	802001	BioLegend	1:1000
βIII-tubulin	Mouse	801202	BioLegend	1:1000
OXT2	Rabbit	AB9566-1	Millipore	1:300
Ki67	Mouse	550609	BD	1:500
SATB2	Mouse	ab51502	Abcam	1:100
Dako Tau	Rabbit	A0024	Dako	1:2000
Tbr1	Rabbit	ab31940	Abcam	1:400
Pax6	Rabbit	901301	Bioligand	1:300
CTIP2	Rat	ab18465	Abcam	1:300

Table 3.
Primary antibodies used for Western blot

Name / Target	Species	Product Code	Company	Dilution
Dako Tau	Rabbit	A0024	Dako	1:2000
HT7	Mouse	MN1000	Thermo	1:1000
S199	Rabbit	ab81268	Abcam	1:1000
S396	Rabbit	ab109390	Abcam	1:1000
AT270	Mouse	MN1050	Thermo	1:1000
PHF1	Mouse	N/A	Peter Davis(48)	1:500
GFAP	Mouse	G6171	SIGMA	1:300
βIII-tubulin	Rabbit	802001	BioLegend	1:1000
βIII-tubulin	Mouse	801202	BioLegend	1:1000
β-Actin	Mouse	A2228	Sigma	1:2000
GAPDH	Mouse	AM4300	Invitrogen	1:1000

Table 4.

Secondary antibodies

Antibody / Use		Species	Product Code	Company	Dilution
Immunoblot Secondary 800nm		Goat anti Rabbit	611-145-122	Rockland	1:20,000
Immunoblot Secondary 680nm		Goat anti Mouse	A21058	Invitrogen	1:20,000
ICC Secondary	568nm	Donkey anti Mouse	A10037	Invitrogen	1:1500
ICC Secondary	568nm	Goat anti Mouse	A21124	Invitrogen	1:1500
ICC Secondary	568nm	Donkey anti Rabbit	A10042	Invitrogen	1:1500
ICC Secondary	488nm	Donkey anti Mouse	A21202	Invitrogen	1:1500
ICC Secondary	488nm	Goat anti Rat	A11006	Invitrogen	1:1500
ICC Secondary	488nm	Goat anti Chicken	A11039	Invitrogen	1:1500
ICC Secondary	488nm	Donkey anti Rabbit	A21204	Invitrogen	1:1500

Figures

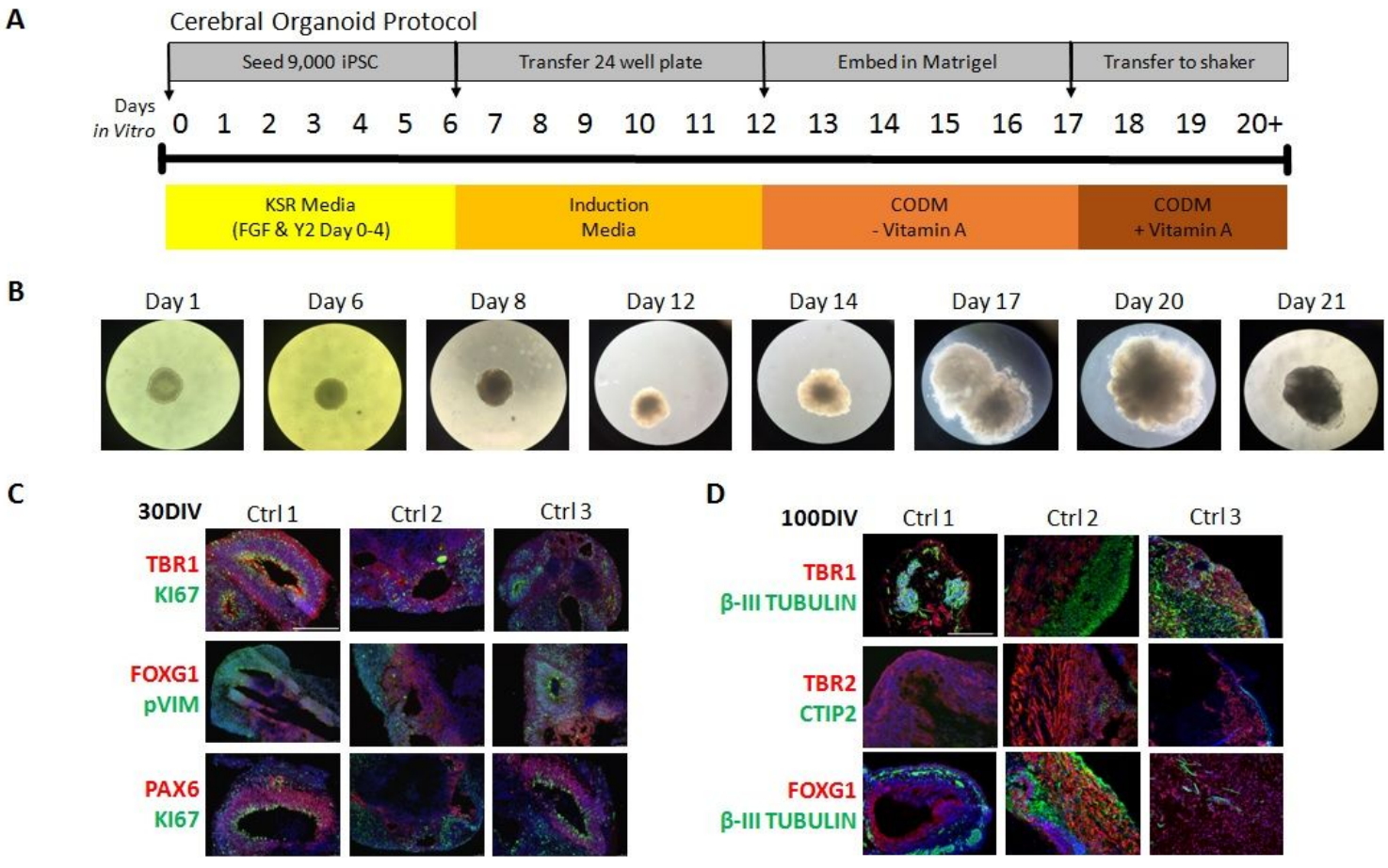

Figure 1

Generation and characterisation of cerebral organoids. A) Simplified schematic of the cerebral organoid (CO) protocol from Lancaster et al, 2014 (27) B) Phase contrast images of cerebral organoids from seeding (Day 1) to 25 DIV. 1-20DIV taken at X10 magnification, 25DIV taken at X4. C) Successful differentiation of 3 control iPSC lines into COs was confirmed by immunocytochemistry after 30 DIV. This confirmed the presence of proliferating precursor cells (Ki67, green), early-born deep-layer neurons (Tbr1, red), neural precursor cells (NPCs) (Pax6, red), radial glia (phospho-Vimentin, green), and neurons of forebrain identity (Foxg1, red). Scale bar 200µm. C) Further characterisation of COs at 100 DIV confirmed the presence of preplate and layer 6 neurons (Tbr1, red), neuronal cells (III-tubulin, green), secondary progenitor cells (Tbr2, red), layer 5 neurons (Ctip2, green) and forebrain neurons (Foxg1, red). Scale bar 200µm.

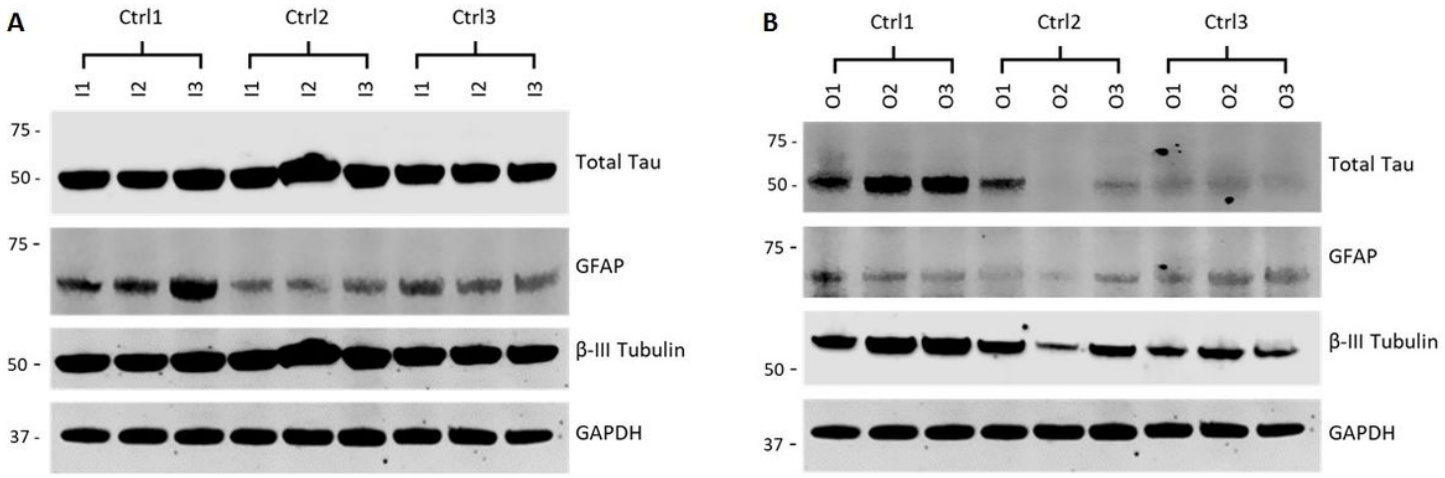

Figure 2

Variability of tau protein levels in COs compared to 2D cortical neurons Western blot analysis of total protein lysates from A) 2D iPSC derived cortical neurons from three inductions (I1, I2, I3) of three independent control iPSC lines (Ctrl 1, Ctrl2, Ctrl3) and B) Three independent COs (O1, O2, O3) from the same three iPSC lines (Ctrl1, Ctrl2, Ctrl3). Membranes were probed for total tau, the astrocyte marker GFAP and pan-neuronal marker β-III tubulin. GAPDH was used as a loading control. All samples were generated at 80 DIV.

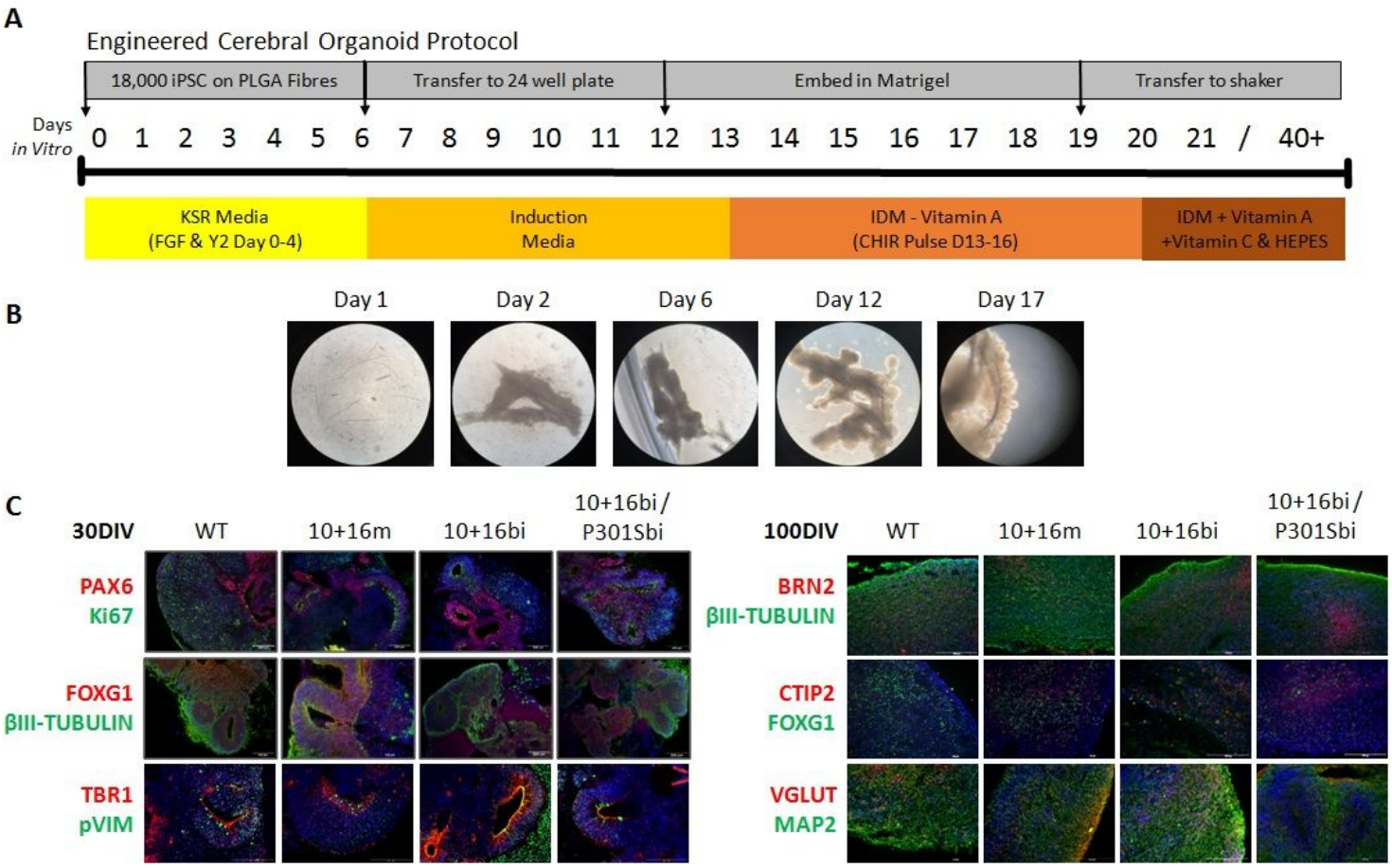

Figure 3

Differentiation of iPSC into engineered cerebral organoids (enCORs). iPSC from WT, 10+16m, 10+16bi and 10+16bi/P301Sbi were used to generate engineered cerebral organoids (enCORs). A) Simplified schematic of the engineered cerebral organoid (enCORs) protocol. B) Phase contrast images of enCORs during early differentiation (1-17 DIV). PLGA fibres within a single cell suspension of iPSC (1 DIV). iPSC cells aggregate around the fibres (2 DIV). Elongated embryoid body (6 DIV). Matrigel embedded enCOR showing formation of cleared neural ectoderm tissue (12 DIV) and neural tube-like structures (17 DIV). C) Successful generation of enCORs was confirmed by immunocytochemistry at 30 DIV. Immunofluorescence confirmed the presence of neural precursor cells (NPCs) (Pax6, red), Proliferating cells (Ki67, green), forebrain-specific markers (Foxg1, red), Neurons (βIII-tubulin), deep layer neurons (Tbr1, red) and radial glia (Phospho-vimentin, green). D) Immunocytochemistry at 100 DIV confirmed the presence of layer II and III neurons (Brn2, red), neurons (βIII-tubulin, green), layer V neurons (Ctip2, red), forebrain-specific markers (Foxg1, green), glutamatergic neurons (Vglut, red) and the pan-neuronal marker (Map2, green).

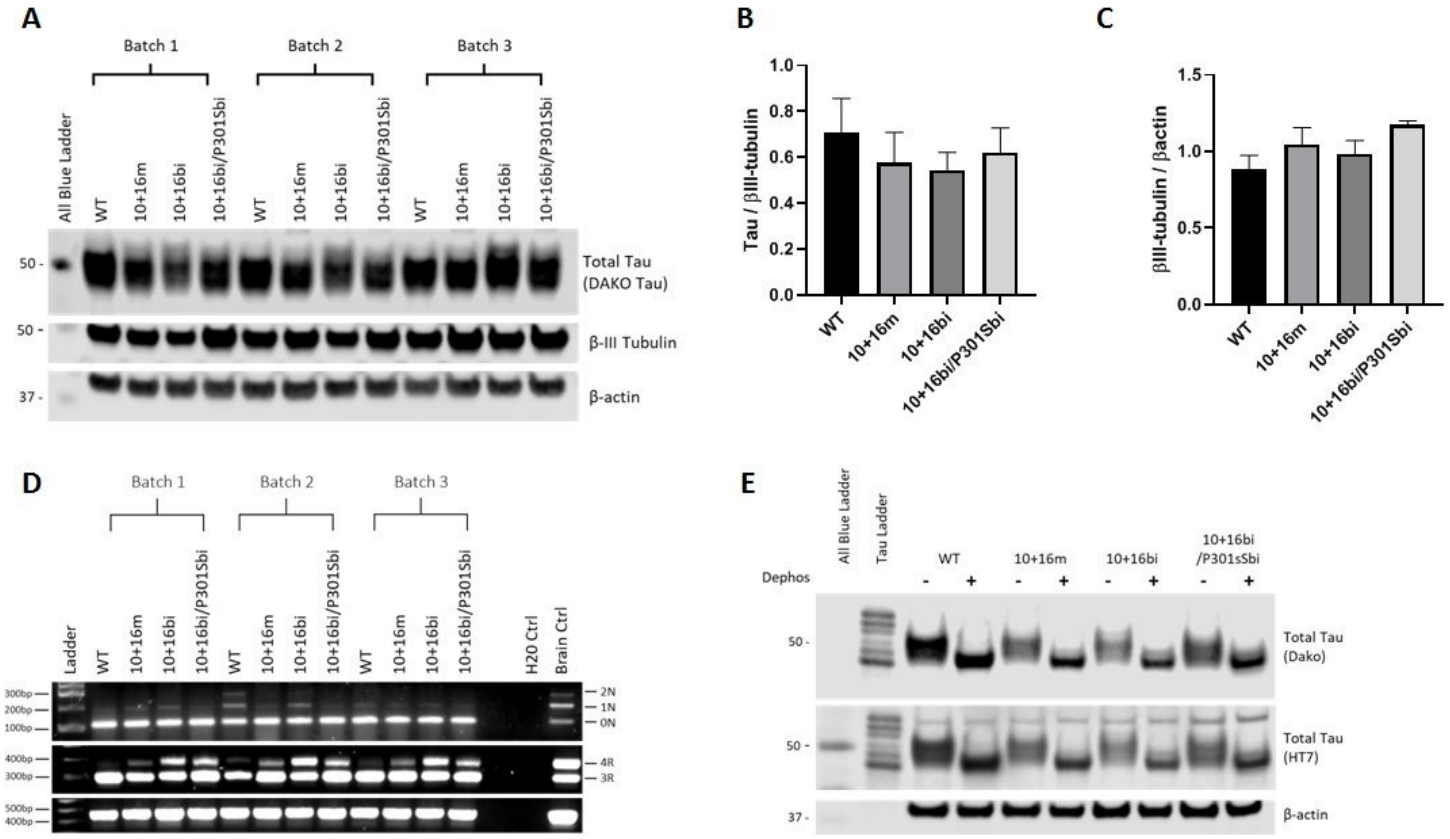

Figure 4

Tau expression and splicing in 100DIV enCORs reveals predominant fetal tau expression A) Three independent batches of enCORs of all four genotypes were analysed by western blot at 100DIV. Membranes were probed for total tau (DAKO) and B-III Tubulin and β-actin. B) Quantification of total tau levels normalised to βIII-tubulin. No significant differences in total tau levels were seen across the isogenic lines or within enCOR batches.C) Quantification of βIII-tubulin levels normalised to β-actin. No significant differences in βIII-tubulin levels were detected across the isogenic lines or within enCOR batches. D) Tau splicing was assessed using primers spanning exons 2 and 3 (0N, 1N, 2N) or primers spanning exon 10 (3R, 4R) of MAPT. 0N, 1N and 2N tau were detected as bands of 112 bp, 199 bp and 286 bp respectively. 3R and 4R tau were detected as products of 305 bp and 398 bp respectively. RNA from human brain tissue was used as a positive control. E) Lysates were either untreated (-) or dephosphorylated with λ-phosphatase (+) prior to gel electrophoresis in order to determine which tau isoforms were present. Membranes were probed with two antibodies to total tau, DAKO and HT7. Recombinant tau ladder was included as a molecular mass control.

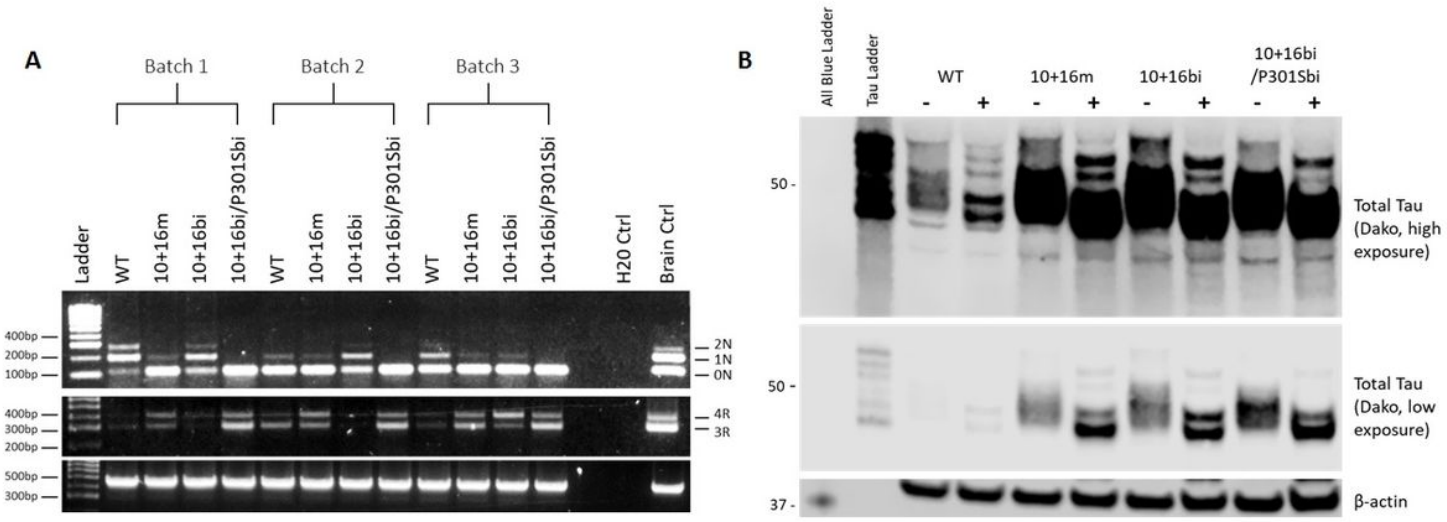

Figure 5

Tau expression and splicing in 200 DIV enCORs A) RT-PCR on 200 DIV samples was used to determine the presence of 0N, 1N and 2N tau transcripts and 3R and 4R tau transcript as described in Fig. 4. Human brain tissue was used as a positive control. B) Western of dephosphorylated lysates from 200DIV enCORs. Lysates treated with (+) and without (-) λ-phosphatase in order to remove phosphate groups from proteins. Total tau was probed for using Dako tau antibody to confirm protein tau isoforms present (Two exposures shown).

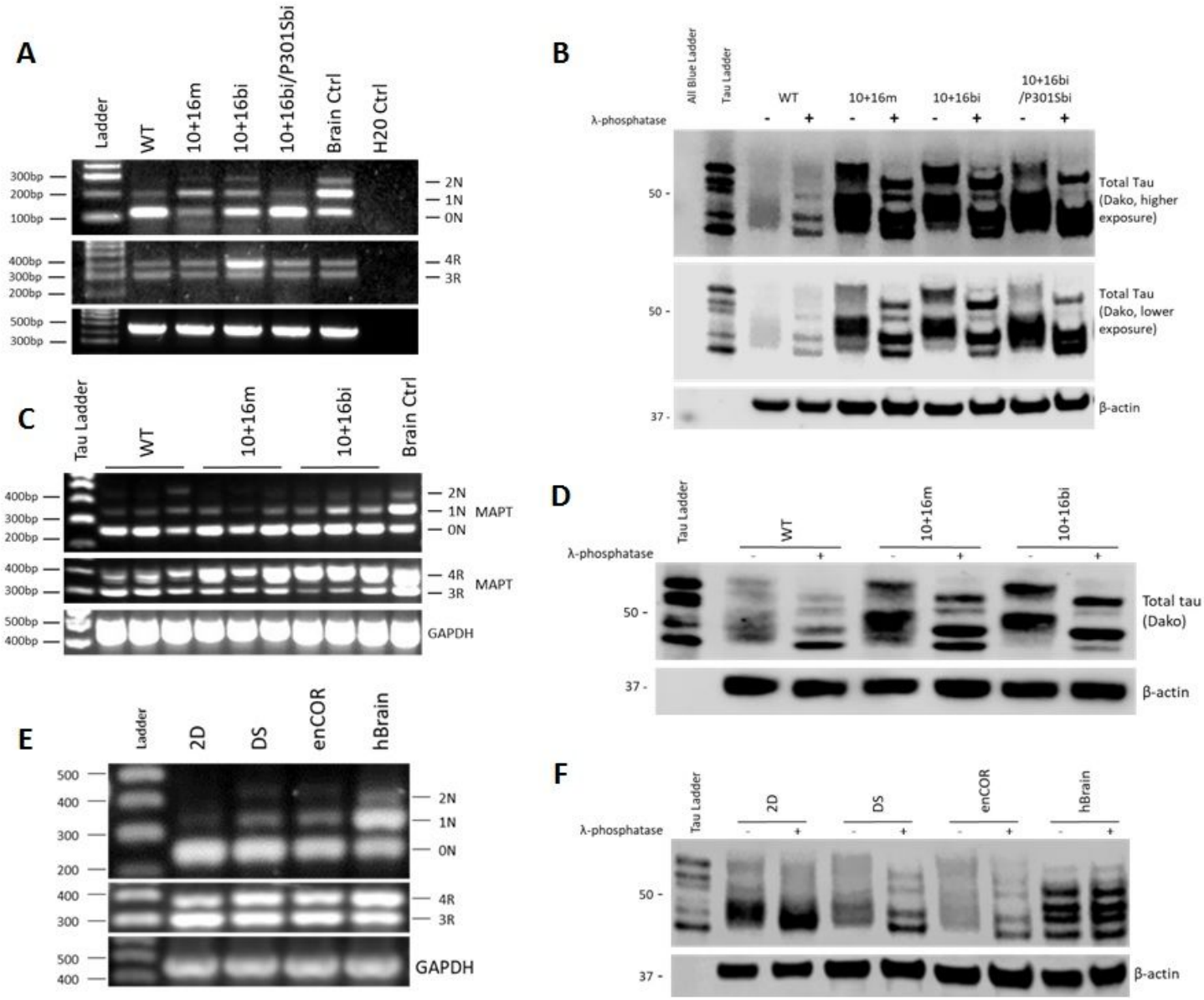

Figure 6

Tau expression and splicing at 300 DIV in multiple differentiation protocols A) RT-PCR was performed on WT and MAPT mutation enCORs at 300 DIV to assess the presence of 0N, 1N and 2N isoforms (upper panel) and 3R and 4R tau (middle panel). GAPDH used as a control (lower panel) B) Western blot of dephosphorylated lysates from 300DIV enCORs. Lysates were treated with (+) and without (-) λ-phosphatase to remove phosphate groups from proteins prior to electrophoresis. Total tau was assessed using DAKO tau antibody to confirm protein tau isoforms present. (Two exposures shown) C) RT-PCR on 300 DIV forebrain organoids from WT and MAPT mutation iPSC was performed to assess levels of 3R and 4R tau, and 0, 1 and 2N tau isoforms. D) 300 DIV forebrain organoid lysates were run with and without λ-phosphatase treatment and then probed for tau. Total tau was assessed using Dako tau antibody and β-actin was used as a loading control. E) RT-PCR with primers spanning MAPT exon 10 was used to assess levels of 3R and 4R tau, and primers spanning Exon 2 and 3 to assess 0, 1 and 2N tau in 2D cortical neurons, enCORs and forebrain organoids.All sample run at 300 DIV againsta human brain sample. F) Tau splicing was assessed by western blot in protein lysates from 2D cortical neurons, encores, forebrain organoids, and post-mortem human brain. All cell lysates were harvested were 300

DIV and samples run with (+) and without (-) prior λ-phosphatase treatment. Total tau was assessed using DAKO tau antibody and β-actin was used as a loading control.

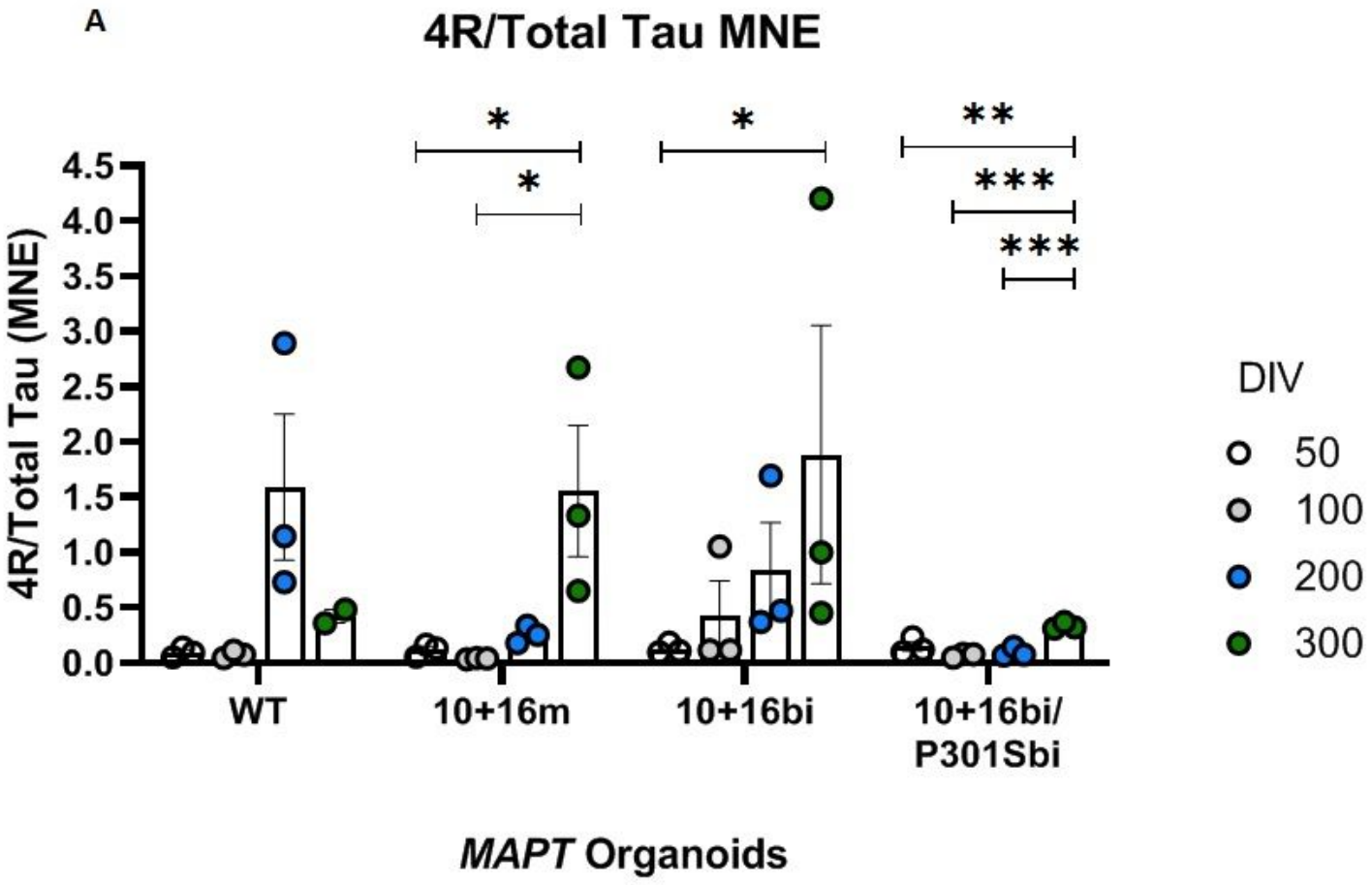

Figure 7

Quantitative assessment of 4R tau isoforms using qPCR enCOR cDNA samples from WT, 10+16m, 10+16bi and 10+16bi/P301Sbiat 50, 100, 200 and 300 DIV, were analysed by qPCR for 4R tau and total tau. Mean normalised expression (MNE) was calculated using MAP2 expression as a pan-neuronal gene. 4R tau was then normalised against total tau.Statistical analysis was performed in Prism using a one-way ANOVA with Tukey's post hoc test: *p < 0.05, ** = < 0.01, *** = < 0.001. n=3 for all samples, except 300 DIV WT, where n=2.

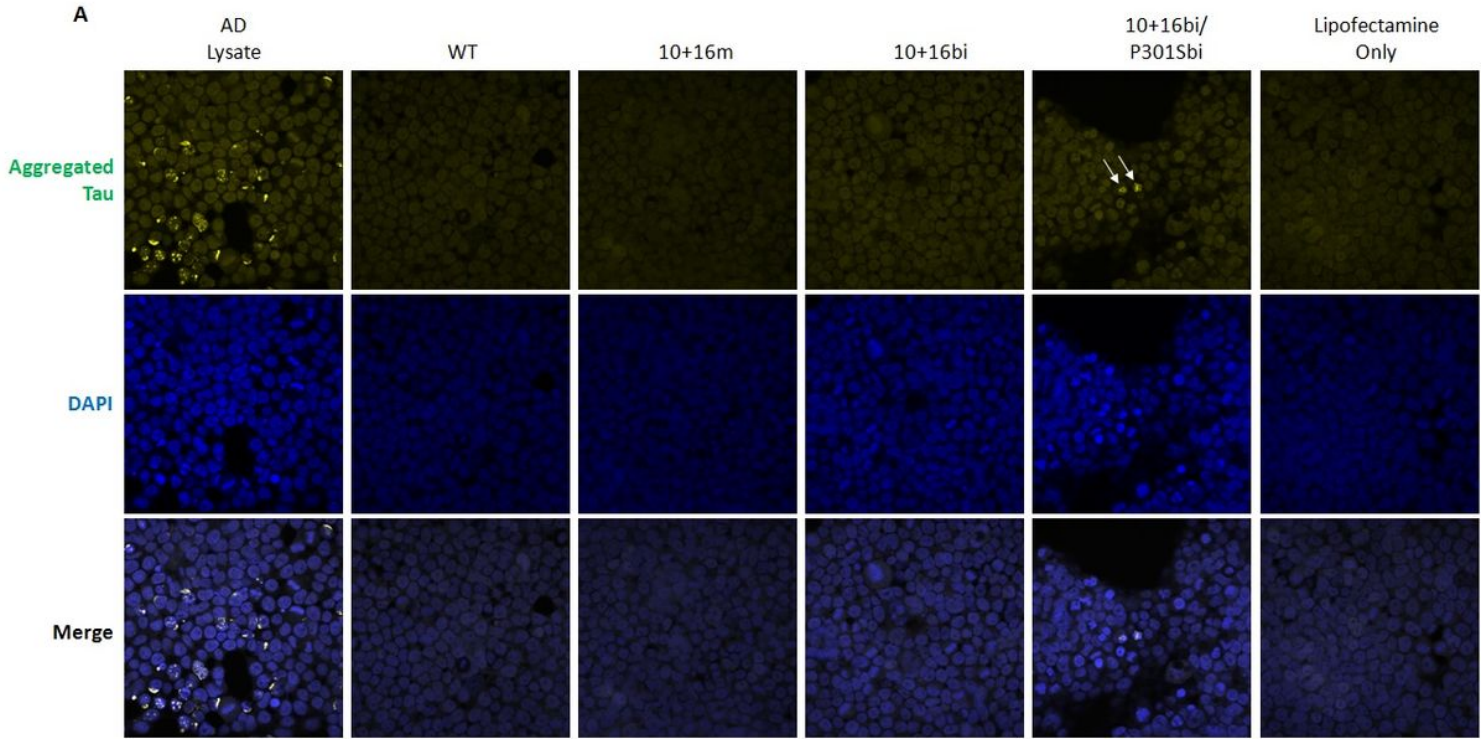

Figure 8

Tau seeding activity of encore extracts at 300 DIV Tau RD P301S FRET Biosensor (ATCC® CRL-3275™) cells were transfected with300 DIV lysates from WT, 10+16m, 10+16bi and 10+16bi/P301Sbi enCORs and imaged 72h post-transfection. AD lysate and lipofectamine only was also transfected as positive and negative controls respectively. AD lysates induce theaggregation ofbiosensor cell line derived fluorescent tau fragments. Cells transfected with 10+16bi/P301Sbi lysates also show tau aggregates (arrows). No seeding activity was detected in lysates from other genotypes.

Supplementary Files

This is a list of supplementary files associated with this preprint. Click to download.

- Supplementaryinformation.docx
- SupplFigures.pptx